

# Generation of High Resolution Handwritten Digits with an Ion-Trap Quantum Computer

Manuel S. Rudolph,<sup>1</sup> Ntwali Toussaint Bashige,<sup>2</sup> Amara Katabarwa,<sup>2</sup>  
Sonika Johri,<sup>3</sup> Borja Peropadre,<sup>2</sup> and Alejandro Perdomo-Ortiz<sup>1,\*</sup>

<sup>1</sup>Zapata Computing Canada Inc., 325 Front St W, Toronto, ON, M5V 2Y1, Canada

<sup>2</sup>Zapata Computing Inc., 100 Federal Street, Boston, MA 02110, USA

<sup>3</sup>IonQ Inc., College Park, MD 20740, USA

(Dated: March 28, 2022)

Generating high-quality data (e.g., images or video) is one of the most exciting and challenging frontiers in unsupervised machine learning. Utilizing quantum computers in such tasks to potentially enhance conventional machine learning algorithms has emerged as a promising application, but poses big challenges due to the limited number of qubits and the level of gate noise in available devices. Here, we provide the first practical and experimental implementation of a quantum-classical generative algorithm capable of generating high-resolution images of handwritten digits with state-of-the-art gate-based quantum computers. In our quantum-enhanced machine learning model, we implement a quantum-circuit based generative model to sample the prior distribution of a Generative Adversarial Network (GAN). We introduce a multi-basis technique which leverages the unique possibility of measuring quantum states in different bases, hence enhancing the expressibility of the prior distribution to be learned. We train of this hybrid algorithm on an ion-trap device based on  $^{171}\text{Yb}^+$  ion qubits to generate high-quality images and quantitatively outperform comparable classical GANs trained on the popular MNIST data set for handwritten digits.

In the last decades, machine learning (ML) algorithms have significantly increased in importance and value due to the rapid progress in ML techniques and computational resources [1, 2]. However, even state-of-the-art algorithms face significant challenges in learning and generalizing from an ever increasing volume of unlabeled data [3–5]. With the advent of quantum computing, quantum algorithms for ML arise as natural candidates in the search of applications of noisy intermediate-scale quantum (NISQ) devices [6], with the potential to surpass classical ML capabilities. Among the top candidates to achieve such a practical quantum advantage in ML are generative models [7], i.e. probabilistic models aiming to capture the most essential features of complex data and to generate similar data by sampling from the trained model distribution. Quantum generative models can provably learn distributions which are outside of classical reach [8–10] and thus offer a new tool set for tackling challenging ML applications, potentially avoiding pitfalls of conventional classical algorithms, improving training and enhancing general performance on generative learning tasks.

Despite this promise, applying and scaling quantum models on small quantum devices to tackle real-world data sets remains a big challenge for quantum ML algorithms. In Ref. [7] it was proposed to leverage state-of-the-art ML techniques to assist the training of quantum models. The idea exploits the known dimensionality-reduction capabilities of deep neural networks [11] to compress classical data before it is handed to a small quantum device. This compressed low-dimensional abstract data is referred to and lives in the so-called *latent space* of the deep network. Having the quantum model learn the latent representation of data and taking part in a joint quantum-classical training loop opens up the possibility for an enhancement of hybrid models

when compared to those consisting of only classical neural networks. This synergistic interaction between the quantum model and the complex classical deep learning algorithm is at the heart of the proposed quantum-assisted Helmholtz machines [7, 12] and more recent hybrid proposals [13, 14] for enhancing Associative Adversarial Networks (AAN) [15]. Both proposals aim to use the quantum model as a way to learn the latent space of their respective neural network model. In the specific case of Ref. [14], the authors propose to use a Quantum Boltzmann Machine (QBM) [16], while Refs. [12, 13] experimentally demonstrated this concept with a D-Wave 2000Q annealing device. A similar adoption of this hybrid strategy with quantum annealers has been explored with variational autoencoders [17]. Despite these efforts, a definite demonstration utilizing truly quantum resources on NISQ devices and with full size ML data sets, e.g. the MNIST data set of handwritten digits [18], has remained elusive to date. Recent experimental results on gate-based quantum computers [19] illustrate such proposals are far from generating high-quality MNIST digits.

In this work, we introduce the Quantum Circuit Associative Adversarial Network (QC-AAN) (see Fig. 1): a framework combining capabilities of NISQ devices with classical deep learning techniques to learn relevant full scale data sets. We apply a Quantum Circuit Born Machine (QCBM) [20] to model and re-parametrize the prior distribution of a Generative Adversarial Network (GAN)[21]. A QCBM is a circuit-based generative model which encodes a data distribution in a quantum state. This approach allows for sampling of the QCBM by repeatedly preparing and measuring its corresponding wavefunction

$$|\psi(\theta)\rangle = U(\theta)|0\rangle. \quad (1)$$

$U(\theta)$  is a parameterized quantum circuit acting on an initial qubit state  $|0\rangle$ , with  $U(\theta)$  chosen according to the capabilities and limitations of NISQ devices. The probabilities of

\* alejandro@zapatacomputing.com

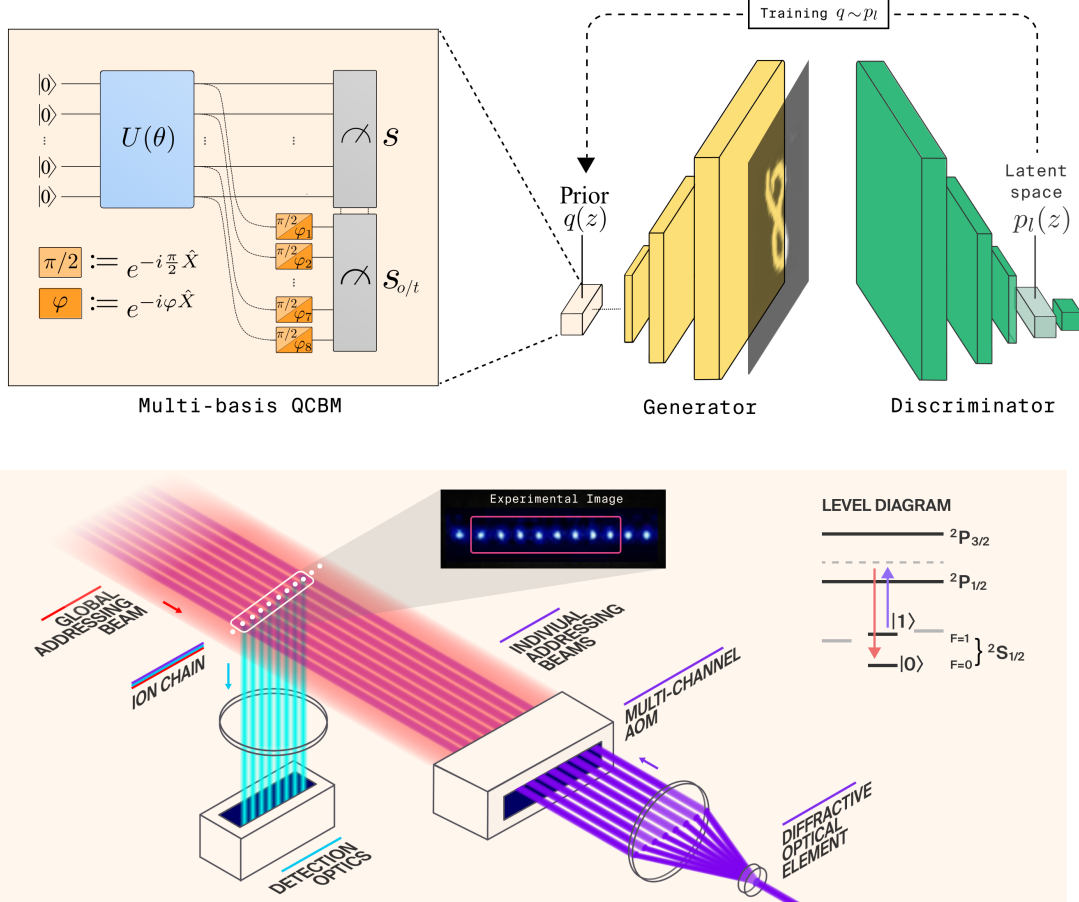


FIG. 1. Top: Schematic description of our Quantum Circuit Associative Adversarial Network (QC-AAN) framework where the prior of a Generative Adversarial Network (GAN) is modelled by a multi-basis Quantum Circuit Born Machine (QCBM). This quantum generative model with encoded distribution  $q(z)$  is trained on latent activations  $\hat{z}$  in layer  $l$  of the discriminator, learning the feature distribution  $p_l$ . In the multi-basis QCBM, trainable single-qubit rotations follow the parametrized quantum circuit  $U(\theta)$  and allow for measuring the prepared wavefunction in additional bases. Angles for those post-rotations can be fixed, e.g. to measure all qubits in the orthogonal  $Y$ -basis, or they can be trained along with other parameters in  $U(\theta)$  to measure  $s_o$  and  $s_t$ , respectively. Measurements  $s$  and  $s_{o/t}$  are concatenated and forwarded as prior samples into the GAN, which is otherwise trained conventionally. To keep consistency with single-qubit gate rotations, we denote  $\hat{X} := \hat{\sigma}_x/2$ . Bottom: Illustration of the 11-qubit ion-trap quantum device by IonQ based on  $^{171}\text{Yb}^+$  ion qubits. The experimental implementation of the QC-AAN algorithm in this work was performed on 8 qubits. The device is operated with automated loading of a linear chain of ions, which is then optically initialized with high fidelity. Computations are performed using a mode-locked 355 nm laser, which drives native single-qubit- and two-qubit gates.

observing any of the  $2^n$  bitstrings  $\mathbf{x}_i$  in the  $n$ -bit (qubit) target distribution probability are modeled using the Born probabilities with  $P(\mathbf{x}_i) = |\langle \mathbf{x}_i | \psi(\theta) \rangle|^2$ . Importantly, QCBMs can be implemented on most NISQ devices (see e.g. Refs. [22–25]) and additionally open our algorithm up to exploit unique features of quantum circuit-based approaches, like the multi-basis technique proposed in this work.

We implement this quantum-classical algorithm experimentally with 8 qubits to generate the first high-resolution handwritten digits with end-to-end training on an ion-trap quantum device. We also argue that implementing a quantum generative model in the prior space of a deep generative neural network could enhance such algorithms by providing

them with non-classical distributions and quantum samples from a variety of measurement bases.

GANs are one of the most popular recent generative machine learning algorithms able to generate remarkably realistic images and other data. In a GAN, a generator  $G$  and a discriminator  $D$  are trained according to the adversarial min-max cost function

$$\mathcal{C}_{GAN} = \min_{G} \max_{D} \left[ \mathbb{E}_{x \sim p_{data}(x)} [\log D(x)] + \mathbb{E}_{z \sim q(z)} [\log (1 - D(G(z)))] \right]. \quad (2)$$

$G$  learns to map prior samples  $z$  from the prior distribution  $q$  to good outputs  $G(z)$  while  $D$  attempts to identify whether

input data is from the training data  $p_{data}$  or if it was generated by  $G$ . The prior of  $G$  is conventionally a high-dimensional continuous uniform or normal distribution with zero mean but discrete Bernoulli priors have also been shown empirically to be competitive [26]. A specific prior distribution should generally be of a shape that allows  $G$  to effectively map it to a high-quality output space while still providing enough edge cases for the model to explore the entire target data space. If the prior space is too small for a given task, the model cannot learn a good approximation of the target data, whereas a large prior requires a notably expressive neural network architecture to be able to map the full space to high-quality outputs [27]. ML practitioners often fall back on utilizing sufficiently large priors and increase the number of parameters in the GAN for their purpose.

Common challenges in training a GAN lie in mode-collapse and non-convergence, which are natural consequences of the delicately balanced adversarial game. Approaches to implement non-trivial priors during training of a GAN, such as the AAN framework, have been suggested to improve training of the algorithm [15, 28]. In an AAN, the prior distribution of  $G$  is re-parametrized by a Restricted Boltzmann Machine (RBM) [29]. This generative model is trained on activations  $\hat{z}$  in the classical layer  $l$  representing the latent space  $p_l$  of  $D$  shown in Fig. 1. The latent space captures features of the training data and generated data which the discriminator  $D$  deems to be important for its classification task. To that end, the GAN cost function in Eq. 2 is extended with the likelihood distance

$$\mathcal{C}_q = \max_q \mathbb{E}_{\hat{z} \sim p_f(\hat{z})} [\log q(\hat{z})] \quad (3)$$

between the current prior distribution  $q$  and the latent space distribution  $p_l$ . This introduces a structure into  $q$  which is specific to the training data set and the current stage of training. RBMs have been shown to be outperformed by comparable QCBM models in learning and sampling probability distributions constructed from real-world data [30]. In our hybrid framework, the prior distribution is modelled by a QCBM that slowly follows changes in the latent space during training of  $G$  and  $D$  in a smooth transition training protocol (see Appendix G) mitigating instabilities in the only-classical AAN (see Appendix H for an example).

Importantly, in this work, we take advantage of an exclusive property of quantum generative models, i.e. their representation of encoded probability distributions in different bases. By training a QCBM on computational basis samples, families of sample distributions, i.e. projections of the wavefunction, become accessible in a range of other basis sets without adding a large number of parameters in the quantum circuit. Thus, we propose a multi-basis technique for the QCBM which provides the QC-AAN with a prior space consisting of quantum samples in flexible bases, potentially enhancing the overall performance of the neural network. Fig. 1 displays how a second set of measurements is prepared in the multi-basis technique by applying parametrized post-rotations to the QCBM wavefunction. Samples of both bases are forwarded through a fully-connected neural network layer and into the generator  $G$  to learn an effective utilization of

Classical Models and MNIST Data		
3 5 1 7 8 0 4 1	8 0 1 2 7 4 5 8	6 3 6 8 7 1 1 0
4 4 8 1 1 8 2 0	9 1 3 1 6 6 3 9	2 0 8 7 7 0 6 3
0 4 9 3 0 9 3 7	4 7 1 1 9 3 6 6	5 4 5 8 9 8 9 6
1 9 1 3 0 7 7 9	9 1 8 8 6 2 9 4	3 7 8 1 5 9 8 0
6 0 5 9 2 0 4 6	1 0 2 5 9 1 5 3	2 7 2 5 3 1 8 7
6 8 0 1 0 2 0 0	9 6 8 3 1 5 7 0	5 8 9 6 1 7 4 1
3 0 7 4 1 1 5 9	5 9 3 8 5 7 7 8	3 7 0 0 7 9 9 2
4 2 4 9 9 0 9 3	6 4 2 3 8 5 5 9	5 9 0 5 9 5 0 4
8 bit DCGAN		16 bit DCGAN
IS = 9.27 ± 0.03		IS = 9.52 ± 0.03
MNIST data		IS = 9.81 ± 0.00
8 Qubit Simulations		
1 6 3 0 4 3 4 7	3 6 2 0 0 1 3 6	0 4 9 3 0 8 9 4
8 7 8 6 0 0 9 8	0 9 2 6 9 5 3 0	3 3 5 1 7 5 1 9
0 1 0 2 1 4 6 0	3 4 6 4 6 4 1 1	6 1 8 8 0 0 7 6
4 1 9 0 1 0 6 6	9 6 1 6 7 1 6 0	8 8 7 1 6 3 4 1
0 4 8 4 0 5 6 9	4 5 5 0 6 2 8 2	8 1 7 8 4 7 1 8
2 4 9 7 0 1 0 3	1 3 5 3 1 6 1 8	2 1 6 7 4 7 4 5
4 4 4 0 1 1 1 6	8 0 1 0 9 0 1 1	1 2 3 0 3 3 4 3
6 0 1 8 8 7 0 1	9 4 6 9 5 7 3 4	1 0 4 3 5 0 1 2
QC-AAN		QC <sub>+</sub> <sub>o</sub> -AAN
IS = 9.33 ± 0.02		IS = 9.59 ± 0.02
QC <sub>+</sub> <sub>t</sub> -AAN		IS = 9.57 ± 0.02

FIG. 2. Digits generated by our QC-AANs with 8 simulated qubits and comparable classical DCGANs. All models shown here were selected among several training repetitions to have a high Inception Score for their respective model type. The multi-basis technique in the QC<sub>+</sub><sub>t</sub>-AAN clearly enhances the algorithm compared to the 8 bit DCGAN and the QC-AAN without measurements in a second basis.

all measurements. The second measurement basis in the multi-basis QCBM can be fixed, for example to measure all qubits in the *orthogonal Y*-basis, or it can be *trained* for each qubit along with other circuit parameters to optimize the information extracted from the quantum state. We call those variants QC<sub>+</sub><sub>o</sub>-AAN and QC<sub>+</sub><sub>t</sub>-AAN, respectively.

As a first step towards showcasing the QC-AAN and our multi-basis technique, we numerically simulate training on the canonical MNIST data set of handwritten digits, a standard data set for benchmarking a variety of ML and deep learning algorithms, using the Orquestra™ platform. To isolate the effect of modelling the prior with a QCBM, we compare our quantum-classical models to purely classical Deep Convolutional GANs (DCGANs) with precisely the same neural network architecture (see Appendix F for details) and with uniform prior distribution. The QCBM is initiated with a warm start such that the prior distribution is uniform and thus QC-AANs and DCGANs are equivalent at the beginning of training. This initialization should additionally avoid complications related to barren plateaus [31]. For more information on the quantum circuit ansatz and training of the QCBM, we refer to Appendix B and Appendix G. To quantitatively assess performance, we calculate the Inception Score (IS) (see Appendix I) which evaluates the quality and diversity of generated images in GANs. The IS is high for a model which produces very diverse images of high-quality handwritten digits.

Fig. 2 shows results of handwritten digits generated by

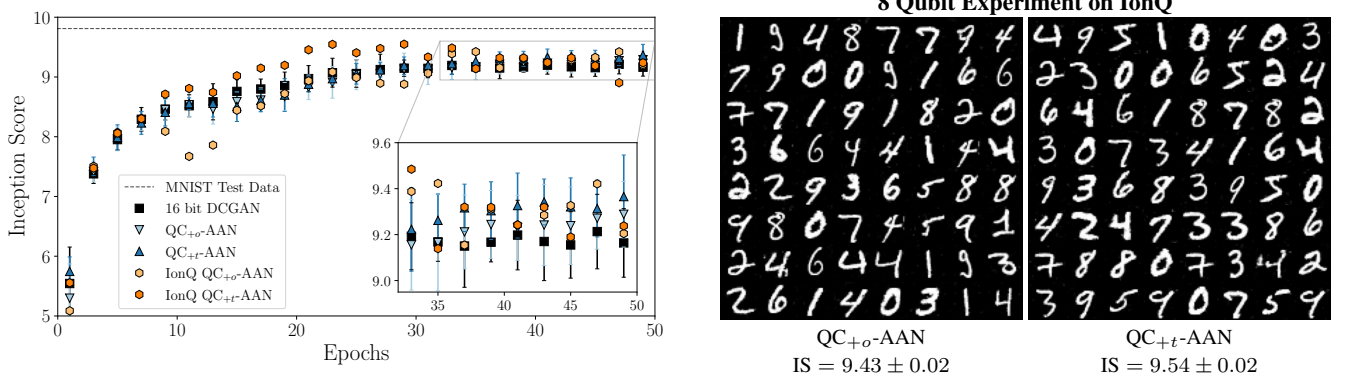


FIG. 3. Left: Quantitative comparison between DCGANs with 16 bit prior distribution and our 8 qubit QC<sub>+o/t</sub>-AAN algorithm. The experimental realization on the IonQ device includes complete implementation of the multi-basis QCBM on hardware. Where present, error bars indicate the standard deviation of 10 independent training repetitions. The 8 qubit hybrid models generally outperform the classical DCGAN with uniform prior distribution. Right: Images of handwritten digits generated by the experimental implementation of the QC<sub>+o/t</sub>-AAN models on the IonQ device. The QC<sub>+o</sub>-AAN model achieves a maximal Inception score of over 9.4 while the QC<sub>+t</sub>-AAN scores over 9.5 with overall better diversity.

our models. For each model type, we pre-selected the best-performing models in terms of the IS and chose a single representative based on quality and diversity of the images for a human observer. The generated digits themselves are random subsamples of the selected models. For details on the training parameters of the QCBM and the neural networks, we refer to Appendix F and Appendix G. It is apparent that all models presented here can potentially achieve good performance and output high-resolution handwritten digits. In a quantitative evaluation of the average model performance (see Appendix E), we see that the 8 qubit QC-AAN without multi-basis technique typically does not outperform comparable 8 bit DCGANs under any of the hyperparameters explored. For low-dimensional priors in general, a uniform prior distribution seems to yield an optimal training for the GAN. In contrast, Fig. 3 shows that both multi-basis QC-AAN models, the QC<sub>+o</sub>-AAN and the QC<sub>+t</sub>-AAN, generate visibly better images and achieve average Inception scores of 9.28 and 9.36, respectively, whereas the DCGAN with 16-dimensional prior averages approximately 9.20. This is a striking result, indicating that an 8 qubit multi-basis QCBM does not require full access to a 16 qubit Hilbert space to outperform a 16 bit DCGAN. Another key observation is that the trained-basis approach generally enhances the algorithm even more compared to the fixed orthogonal-basis approach.

To provide final confirmation that the QC-AAN framework is fit for implementation on NISQ devices, we train the QC<sub>+o/t</sub>-AAN algorithms on a quantum device from IonQ which is based on <sup>171</sup>Yb<sup>+</sup> ion qubits. For more information on the device, we refer to Fig. 1, Appendix A, and Ref. [32]. The experimental results for the full training *on hardware* can be viewed in Fig. 3. To the best of our knowledge, this is the first practical implementation of a quantum-classical algorithm generating high-resolution digits on a NISQ device. With as few as 8 qubits, we show signs of positively influencing the training of GANs, indicating general utility in mod-

elling their prior with a QCBM on NISQ devices and a potential quantum enhancement by utilizing quantum samples in several bases. Learning the choice of the second measurement basis through the quantum-classical training loop, i.e. our QC<sub>+t</sub>-AAN algorithm, appears to be the most successful algorithm in simulations and also in the experimental realization on the IonQ device. This is a great example of how quantum components in a hybrid quantum ML algorithm are capable of effectively utilizing feedback coming from classical neural networks and a testament to the general ML approach of learning the best parameters rather than fixing them. Unlike many other use-case implementations of quantum algorithms on NISQ devices, our models do not under-perform compared to noise-free simulations. It is reasonable that significant reparametrization of the prior space, paired with a modest noise floor, provide GANs with an improved trade-off between exploration of the target space and convergence to high-quality data.

Using a quantum generative model like a QCBM as a building block in the prior space of larger classical generative ML models, unlocks the path to effectively studying the influence of certain prior shapes on a given learning task. This is a field which is worth studying in the context of deep learning algorithms [26], and a quantum model may offer the tools required to do so. Our QC-AAN framework flexibly extends to more complex datasets such as larger and colored images for which we expect refinement of the prior distribution to become more vital for performance of the algorithm. Besides extending to these more challenging datasets, we could adapt the learning strategy of the quantum prior to follow a different objective function, potentially one that directly ties into improving the generator's performance in the adversarial game with the discriminator. Exploring prior distributions from quantum-inspired models such as the tensor-network-based Born machines [33] is another exciting research direction we will be exploring.

Given that our multi-basis technique equips hybrid

quantum-classical algorithms with quantum samples which could enhance deep learning models beyond a classical threshold, it is essential that we better understand the kinds of quantum distributions that can be built from these families of basis set measurement distributions. Despite the enhancement observed in our hybrid quantum models, it is not the intention of this work to claim a quantum advantage. A full-fledged quantitative comparison between quantum and classical versions of machine learning algorithms can be challenging. For instance, classical resources are currently much cheaper and more accessible than quantum resources. Therefore, our focus has been towards showcasing our quantum-assisted algorithm which is able to outperform comparable classical GANs on the MNIST data set of handwritten digits. Although for this task, one might be able to achieve better classical ML performance by choosing more sophisticated variants of GANs, we show that our QC-AAN framework could be a strong candi-

date to potentially enhance the best classical GANs with NISQ devices on full scale data sets.

## ACKNOWLEDGMENTS

The authors would like to thank Coleman Collins and Algert Sula for their support with the experimental images and the design of the hardware illustrations. The authors also thank Yudong Cao, Max Radin, Marta Mauri, Matthew Beach, and Dax Enshan Koh for their feedback on an early version of this manuscript. The authors would like to acknowledge Zapata Computing’s Platform Team for all the support with Orquestra™: the software platform used during the execution of all the simulations and experiments shown here. M.R would like to acknowledge Zapata Computing for hosting his Quantum Applications Internship.

---

[1] Yann LeCun, Yoshua Bengio, and Geoffrey Hinton, “Deep learning,” *Nature* **521**, 436 – 444 (2015).

[2] Jürgen Schmidhuber, “Deep learning in neural networks: An overview,” *Neural Networks* **61**, 85 – 117 (2015).

[3] Y. Cheng, D. Wang, P. Zhou, and T. Zhang, “Model compression and acceleration for deep neural networks: The principles, progress, and challenges,” *IEEE Signal Processing Magazine* **35**, 126–136 (2018).

[4] Roman Novak, Yasaman Bahri, Daniel A. Abolafia, Jeffrey Pennington, and Jascha Sohl-Dickstein, “Sensitivity and generalization in neural networks: an empirical study,” (2018), arXiv:1802.08760 [stat.ML].

[5] Behnam Neyshabur, Zhiyuan Li, Srinadh Bhojanapalli, Yann LeCun, and Nathan Srebro, “The role of over-parametrization in generalization of neural networks,” in *International Conference on Learning Representations* (2019).

[6] John Preskill, “Quantum computing in the NISQ era and beyond,” *Quantum* **2**, 79 (2018).

[7] Alejandro Perdomo-Ortiz, Marcello Benedetti, John Realpe-Gómez, and Rupak Biswas, “Opportunities and challenges for quantum-assisted machine learning in near-term quantum computers,” *Quantum Science and Technology* **3**, 030502 (2018).

[8] Yuxuan Du, Min-Hsiu Hsieh, Tongliang Liu, and Dacheng Tao, “The expressive power of parameterized quantum circuits,” arXiv preprint arXiv:1810.11922 (2018).

[9] Ivan Glasser, Ryan Sweke, Nicola Pancotti, Jens Eisert, and J. Ignacio Cirac, “Expressive power of tensor-network factorizations for probabilistic modeling, with applications from hidden Markov models to quantum machine learning,” arXiv:1907.03741v2 (2019).

[10] Ryan Sweke, Jean-Pierre Seifert, Dominik Hangleiter, and Jens Eisert, “On the quantum versus classical learnability of discrete distributions,” (2020), arXiv:2007.14451 [quant-ph].

[11] Geoffrey E Hinton and Ruslan R Salakhutdinov, “Reducing the dimensionality of data with neural networks,” *Science* **313**, 504–507 (2006).

[12] Marcello Benedetti, John Realpe-Gómez, and Alejandro Perdomo-Ortiz, “Quantum-assisted Helmholtz machines: A quantum-classical deep learning framework for industrial datasets in near-term devices,” *Quantum Science and Technology* **3**, 034007 (2018).

[13] Max Wilson, Thomas Vandal, Tad Hogg, and Eleanor Gilbert Rieffel, “Quantum-assisted associative adversarial network: Applying quantum annealing in deep learning,” *CoRR* (2019), arXiv:1904.10573.

[14] Eric R. Anschuetz and Cristian Zanoci, “Near-term quantum-classical associative adversarial networks,” *Physical Review A* **100** (2019).

[15] Tarik Arici and Asli Celikyilmaz, “Associative adversarial networks,” *CoRR* (2016), arXiv:1611.06953.

[16] Mohammad H. Amin, Evgeny Andriyash, Jason Rolfe, Bohdan Kulchytskyy, and Roger Melko, “Quantum Boltzmann machine,” (2016), arXiv:1601.02036.

[17] Walter Vinci, Lorenzo Buffoni, Hossein Sadeghi, Amir Khoshman, Evgeny Andriyash, and Mohammad Amin, “A path towards quantum advantage in training deep generative models with quantum annealers,” *Machine Learning: Science and Technology* (2020).

[18] Y. Lecun, L. Bottou, Y. Bengio, and P. Haffner, “Gradient-based learning applied to document recognition,” *Proceedings of the IEEE* **86**, 2278–2324 (1998).

[19] He-Liang Huang *et al.*, “Experimental quantum generative adversarial networks for image generation,” (2020), arXiv:2010.06201 [quant-ph].

[20] Marcello Benedetti, Delfina Garcia-Pintos, Oscar Perdomo, Vicente Leyton-Ortega, Yunseong Nam, and Alejandro Perdomo-Ortiz, “A generative modeling approach for benchmarking and training shallow quantum circuits,” *npj Quantum Information* **5**, 45 (2019).

[21] Ian Goodfellow, Jean Pouget-Abadie, Mehdi Mirza, Bing Xu, David Warde-Farley, Sherjil Ozair, Aaron Courville, and Yoshua Bengio, “Generative adversarial nets,” in *Advances in Neural Information Processing Systems 27*, edited by Z. Ghahramani, M. Welling, C. Cortes, N. D. Lawrence, and K. Q. Weinberger (Curran Associates, Inc., 2014) pp. 2672–2680.

[22] Kathleen E. Hamilton, Eugene F. Dumitrescu, and Raphael C. Pooser, “Generative model benchmarks for superconducting qubits,” arXiv preprint arXiv:1811.09905 (2018).

[23] Vicente Leyton-Ortega, Alejandro Perdomo-Ortiz, and Oscar Perdomo, “Robust implementation of generative modeling with parametrized quantum circuits,” arXiv preprint

arXiv:1901.08047 (2019).

[24] Brian Coyle, Maxwell Henderson, Justin Chan Jin Le, Niran Kumar, Marco Paini, and Elham Kashefi, “Quantum versus classical generative modelling in finance,” (2020), arXiv:2008.00691 [quant-ph].

[25] D. Zhu, N. M. Linke, M. Benedetti, K. A. Landsman, N. H. Nguyen, C. H. Alderete, A. Perdomo-Ortiz, N. Korda, A. Garfoot, C. Brecque, L. Egan, O. Perdomo, and C. Monroe, “Training of quantum circuits on a hybrid quantum computer,” arXiv preprint arXiv:1812.08862 (2018).

[26] Andrew Brock, Jeff Donahue, and Karen Simonyan, “Large scale GAN training for high fidelity natural image synthesis,” (2019), arXiv:1809.11096 [cs.LG].

[27] Manisha Padala, Debojit Das, and Sujit Gujar, “Effect of input noise dimension in GANs,” (2020), arXiv:2004.06882 [cs.LG].

[28] Thomas Goerttler and Marius Kloft, “Learning a multimodal prior distribution for generative adversarial nets,” (2019).

[29] David H Ackley, Geoffrey E Hinton, and Terrence J Sejnowski, “A learning algorithm for Boltzmann machines,” *Cognitive science* **9**, 147–169 (1985).

[30] Javier Alcazar, Vicente Leyton-Ortega, and Alejandro Perdomo-Ortiz, “Classical versus quantum models in machine learning: insights from a finance application,” *Machine Learning: Science and Technology* **1**, 035003 (2020).

[31] Jarrod McClean, Sergio Boixo, Vadim Smelyanskiy, Ryan Babbush, and Hartmut Neven, “Barren plateaus in quantum neural network training landscapes,” *Nature Communications* **9** (2018).

[32] K. Wright *et al.*, “Benchmarking an 11-qubit quantum computer,” *Nature Communications* **10** (2019), 10.1038/s41467-019-13534-2.

[33] Song Cheng, Jing Chen, and Lei Wang, “Information perspective to probabilistic modeling: Boltzmann machines versus Born machines,” *Entropy* **20** (2017).

[34] James C Spall *et al.*, “Multivariate stochastic approximation using a simultaneous perturbation gradient approximation,” (1992).

[35] Ali Borji, “Pros and cons of GAN evaluation measures,” *Computer Vision and Image Understanding* **179**, 41–65 (2019).

[36] C. Szegedy, V. Vanhoucke, S. Ioffe, J. Shlens, and Z. Wojna, “Rethinking the inception architecture for computer vision,” in *2016 IEEE Conference on Computer Vision and Pattern Recognition (CVPR)* (2016) pp. 2818–2826.

## Appendix A: Details on the IonQ Hardware

The experimental circuits are implemented on an 11-qubit trapped ion processor based on  $^{171}\text{Yb}^+$  ion qubits. The hyperfine levels of the  $^2S_{1/2}$  ground state are used as the states of the qubit with  $|0\rangle = |F = 0, m_F = 0\rangle$  and  $|1\rangle = |F = 1, m_F = 0\rangle$ . Measurement of the entire qubit register is achieved through state dependent fluorescence between  $|1\rangle$  and  $^2P_{1/2}$  states, with the scattered photons being collected through an aperture lens and passed through a dichroic mirror to an array of photon detectors.

The 11-qubit device is operated with automated loading of a linear chain of ions, which is then optically initialized with high fidelity. Computations are performed using a mode-locked 355nm laser, which drives native single-qubit-gate (SQG) and two-qubit-gate (TQG) operations. TQG operations are done through the motional modes shared by all the ions,

this allows for an all to all connectivity topology. The native entangling operation, the Mølmer Sørenson gate, written using Pauli operators is

$$\theta_{xx}^{i,j} = e^{-i\frac{\theta}{2}\sigma_x^i\sigma_x^j}. \quad (\text{A1})$$

In order to maintain consistent gate performance, calibrations of the trapped ion processor are automated. Additionally, phase calibrations are performed for SQG and TQG sets, as required for implementing computations in queue and to ensure consistency of the gate performance.

The device is commercially available through IonQ’s cloud service. On the cloud, the system has all-to-all connectivity, an average 1-qubit gate fidelity of 99.35%, 2-qubit gate fidelity  $> 98\%$  and SPAM error of 99.3%. The error per gate is less than  $4 \times 10^{-3}$ . For more details we refer to Ref. [32].

## Appendix B: The Quantum Circuit Born Machine

Fig. 4 shows the quantum circuit ansatz used throughout this work to implement the QCBM state preparation unitary  $U$  such that

$$|\psi(\theta)\rangle = U(\theta)|0\rangle. \quad (\text{B1})$$

The ansatz is inspired by capabilities of current ion-trap quantum devices and is structured in layers where expressivity of the model increases as layers are added. Although the QCBM equipped with this ansatz can become a powerful generative model, one needs to consider important trade-offs in the ansatz hyperparameter choice. For NISQ quantum devices, shallow quantum circuits are generally desired as deeper circuits can significantly decrease fidelity of the quantum states. Additionally, deep circuits oftentimes come with an excess number of parametrized quantum gates that enhance expressivity but can compromise trainability as well as creating a model that strongly overfits training data. For our work, we limit ourselves to 2 layers to minimize the number of gates used while introducing entanglement into the quantum state. Additionally, we reduce the all-to-all connectivity of the  $XX$  gates shown in Fig. 4 to a linear chain of entangling operations for the experiment on the IonQ quantum device. The circuit parameters are initialized with a warm start such that the QCBM encodes a uniform distribution in computational basis as well as the  $o/t$  bases discussed in the main text and Appendix C.

In our application, the QCBM is trained by minimizing the *clipped negative log-likelihood*

$$\mathcal{L}(\theta) = - \sum_x p(\mathbf{x}) \log \max(q_\theta(\mathbf{x}), \epsilon) \quad (\text{B2})$$

where  $p(\mathbf{x})$  is the probability over  $N$  training data samples  $\mathbf{x}$  and  $q_\theta(\mathbf{x}) = |\langle \mathbf{x} | \psi(\theta) \rangle|^2$  is the QCBM model distribution. A regularization constant  $\epsilon$  prevents singularity of the logarithm for samples with zero probability. The probability distribution  $q_\theta(\mathbf{x})$  of samples  $\mathbf{x}$  is estimated by sampling the prepared state and accumulating the measurements

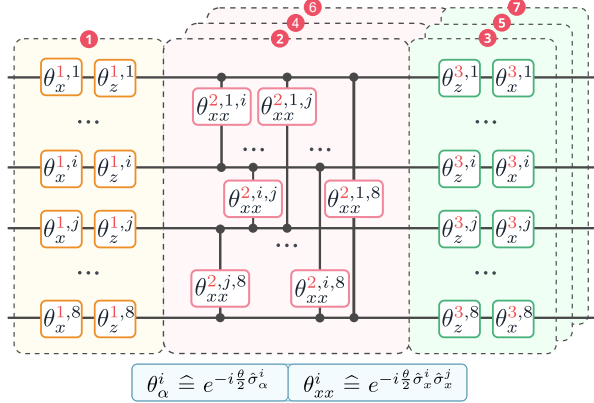


FIG. 4. Quantum circuit ansatz for the QCBM. The ansatz is structured in layers to control expressivity of the model and fidelity of the prepared state. Throughout this work, we use a layer depth of 2 in order to maximize fidelity in the experimental implementation and enforce some interpolation between learned samples. The red numbers indicate the layer counting convention. For simulations, we used the all-to-all entangling layer as shown here, whereas for the experimental implementation, we instead adopted linear nearest-neighbor connectivity.

### Appendix C: The Multi-Basis Technique

In this work, we introduce a multi-basis technique for quantum circuit-based models to expand the repertoire of quantum machine learning researchers. It can aid algorithms to gain a practical quantum advantage by providing it with quantum samples in different measurements bases which have no classical analog.

Commonly, when referring to *sampling* a generative model, one means generating instances of data that follow the encoded probability distribution. For classical models, one is limited to one basis - the computational basis. In quantum models, this is not the case. When encoding a probability distribution into a qubit wavefunction, as is the case with a Quantum Circuit Born Machine (QCBM), the learned wavefunction contains a potential family of sample distributions which are accessible by measuring in different bases. These additional distributions, or more specifically, projections of the wavefunction, can be evaluated by applying arbitrary post-rotations to the quantum registers before measurement. In this work, we explore the questions of whether we can enhance a generative model by including measurements in additional bases and how we can maximize the benefit of measuring additional basis sets. For the selection of the measured bases, we follow an ML approach where we train the post-rotation angles together with the parameters for the ansatz to learn a more flexible prior. This is done by doubling the latent space in the discriminator and training the samples of the multi-basis QCBM on its activations.

When measuring the multi-basis QCBM wavefunction in Eq. B1, we obtain a sample  $\mathbf{s}$  in computational basis, the Z-basis. Other basis measurements are prepared by

applying parametrized single qubit rotations  $R_X(\varphi_i)$  for each qubit  $i$ . For  $\varphi = \pi/2$ , the state gets rotated into the Y-basis, which we refer to as the ‘orthogonal basis’ and is denoted with  $o$  throughout this work. The general case of  $\varphi$  defines what we call the ‘trained basis’ which we denote with  $t$ . When preparing the same QCBM wavefunction and applying the corresponding single-qubit post-rotations, we obtain a sample  $\mathbf{s}_{o/t} \in \{0, 1\}^n$  in the orthogonal or trained basis, respectively. By concatenating the samples  $\mathbf{s}_z$  and  $\mathbf{s}_{o/t}$  into an extended sample  $\mathbf{s}^* = \mathbf{s} \circ \mathbf{s}_{o/t}$ , we can leverage information that is present in the model but conventionally not used. As an explicit example, samples  $\mathbf{s} = 1010$  and  $\mathbf{s}_{o/t} = 1100$  in computational and  $o/t$  basis, respectively, then define  $\mathbf{s}^* = 10101100$ . For a series of measurements in the computational and  $o/t$  bases, the assignment of which pair of measurements is forwarded to the neural network is arbitrary as there is no direct correlation between the computational basis and  $o/t$  basis distributions other than that they obey the normalization constraint of the QCBM wavefunction. This technique generalizes to the measurement and concatenation of samples of any observable able to be measured on a quantum device.

A more subtle advantage of this multi-basis technique in the context of generative modelling with a QCBM is that the dimension of the effective sample space for  $n$  qubits increases from  $2^n$  to  $2^{2n}$ . Although the sample  $\mathbf{s}^*$  lives in the  $\{0, 1\}^{2n}$  space, the multi-basis QCBM does not have access to the full  $2n$  qubit space because of the normalization constraint of the wavefunction. However, increasing the sample dimension and additionally the amount of information encoded and utilized from small near-term quantum computers, here proved of immense value by enhancing the expressivity and the robustness of the hybrid QC-AAN model considered. In principle, we could construct multiple basis sets with few additional gates and a linear scaling in the number of state-preparations, although this implies measuring increasingly redundant bases. The optimal number of basis sets likely depends on the given learning task and available resources.

### Appendix D: Associative Adversarial Networks

Associative Adversarial Networks (AANs) were first proposed in Ref. [15] as an extension of the popular Generative Adversarial Networks (GANs). Their purpose was to improve trainability and consequently general performance of GANs by modeling and reparametrizing the generator  $G$ ’s prior distribution with a restricted Boltzmann machine (RBM). The objective functional for the AAN is

$$\mathcal{C}_{AAN} = \mathcal{C}_{GAN} \circ \mathcal{C}_q, \quad (D1)$$

and consists of the traditional minimax game objective of a GAN

$$\mathcal{C}_{GAN} = \min_G \max_D \left[ \langle \log D(\mathbf{x}) \rangle_{\mathbf{x} \in \text{data}} + \langle \log(1 - D(G(\mathbf{z}))) \rangle_{\mathbf{z} \in q} \right], \quad (D2)$$

and the cost function for the RBM

$$\mathcal{C}_q = \max_q \langle \log q(\hat{\mathbf{z}}) \rangle_{\hat{\mathbf{z}} \sim p_l}, \quad (\text{D3})$$

which maximized the likelihood distance of the RBM distribution

$$q(\mathbf{z}) = \sum_{\mathbf{h}} \frac{e^{-E(\mathbf{z}, \mathbf{h})}}{Z}, \quad (\text{D4})$$

and the latent distribution  $p_l$  in the discriminator  $D$ .  $E(z, h)$  is the energy functional for the RBM with visible units  $\mathbf{z}$  and hidden units  $\mathbf{h}$ , and  $Z = \sum_{\mathbf{z}, \mathbf{h}} e^{-E(\mathbf{z}, \mathbf{h})}$  is the partition function. For more details, we refer the reader to the original AAN paper in Ref. [15].

### Appendix E: Simulated QC-AAN results for 6 and 8 qubits

To benchmark the performance of a QC-AAN with few qubits, we compare average Inception Scores (IS) of our QC-AANs, with 6- and 8-qubit multi-basis QCBM in the model prior. For this work, we only compare models with the same prior dimension to isolate the effect that re-parametrization of the prior distribution has on GAN training. In Fig. 5 we show that for 6- and 8-qubit QC-AANs, we could not achieve an advantage in learning a non-trivial prior. For a 6 (8) qubit QCBM, there are only 64 (256) distinct samples available for the neural network to map to high-quality images. Since the IS is very sensitive to class imbalance of the generated images, we see that modeling those priors does not lead to meaningful improvements. In fact, the results shown in Fig. 5 for the QC-AAN with 6- and 8 qubits were obtained by only minimally disturbing the uniform distribution. The QC<sub>+/o/t</sub>-AANs with the multi-basis technique show interesting results where for 6 qubits, we almost reach the performance of a 12 bit DCGAN, whereas with 8 qubits, we outperform a 16 bit DCGAN (see Fig. 3 in main text). This is despite the fact that the QC<sub>+/o/t</sub>-AAN models are restricted to an effective sub-space compared to a Hilbert space with double the number of qubits.

Note, that these results are specific to our neural network architecture. It is possible that more expressive and computationally intensive neural networks face less challenges in learning a great model with a uniform prior distribution. For a general learning task and network architecture, the QC-AAN algorithm allows to consider the hyperparameters of the trainable prior as hyperparameters towards a more successful overall generative algorithm.

The 8 qubit QC<sub>+/o/t</sub>-AANs operate on a space with  $2^{16} = 65,536$  potential samples. Although the multi-basis QCBM is a binary model, with this amount of different images, an Inception Score of occasionally over 9.5 can be considered to be comparable to state-of-the-art GANs with continuous priors. In fact, Ref. [26] argues that binary units may perform at least as good as continuous uniform or normal distributions.

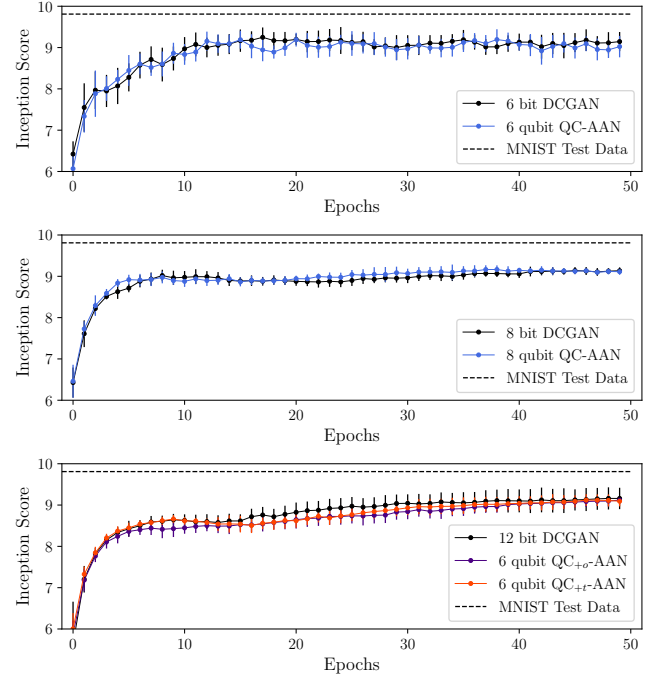


FIG. 5. Simulation results of QC-AANs with 6- and 8 qubits relative to comparable DCGANs with uniform prior distribution. Depicted are average Inception Scores and standard deviations of 10 independent training repetitions per model. We observe no significant improvement for the 6- and 8 qubit QC-AANs, as well as for the QC<sub>+/o/t</sub>-AANs with 6 qubits. For results of the 8 qubit QC<sub>+/o/t</sub>-AAN, we refer to Figure 3 in the main text.

### Appendix F: Neural Network Architectures and Training

Fig. 6 shows the network architectures of generator  $G$  and discriminator  $D$  in this work for our hybrid QC-AANs and the classical DCGANs. They have approximately inverse structure with three convolutional layers, although it is not generally required for stable GAN training. The second to last layer in  $D$  (latent space) has the same size as the first layer in  $G$  (prior space) to be able to train the quantum model in the QC-AAN on the latent activations of  $D$ . The total number of parameters in each network amounts to approximately  $2.77 \times 10^5$ . The multi-basis QCBM in the QC-AAN adds between 31 and 52 trainable parameters for the 8 qubit model, equating to an increase of 0.02% in the total number of parameters.

All convolutional layers have batch normalization and *leaky ReLU* activation functions. In training  $D$ , a small percentage (3%) of training samples have their label flipped and label smoothing is applied to the training images. The optimizer for both networks is the ADAM optimizer with parameters  $[\beta_1, \beta_2] = [0.5, 0.9]$ .

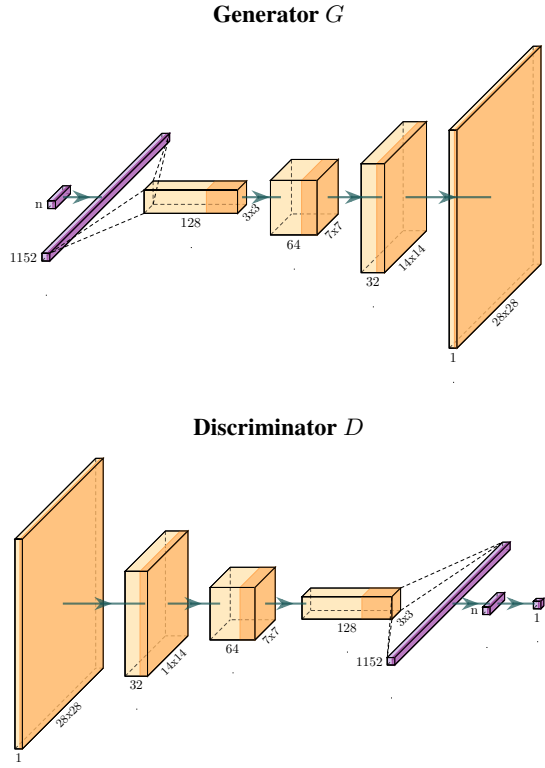


FIG. 6. Schematic neural network architectures of the generator  $G$  and discriminator  $D$  used throughout this work for the MNIST dataset of handwritten Digits. Purple color indicate a 1d layer of nodes whereas the orange blocks represent 2d convolutional layers with 128, 64 and 32 channels.  $G$  and  $D$  are approximately inverse, although this is not strictly required. Note that the second to last layer in  $D$  represents the latent space which contains  $n$  bits, the same size chosen for the prior of  $G$ .

#### Appendix G: Training Details of the QCBM as Model Prior

The QCBM in this work implements a hardware efficient ansatz inspired by capabilities of ion-trap quantum computers (see Fig. 4). The layer depth of the ansatz is chosen to be shallow with only one layer of single-qubit and entangling gates respectively. For the numerical simulations, we chose an all-to-all connectivity between qubits, whereas in the hardware implementation, we used linear connectivity to improve the state fidelity. For the case of the MNIST training set, we did not observe on average significant negative effects in reducing the ansatz connectivity. We expect that for more challenging generative modeling tasks, the circuit ansatz will play a more crucial role.

Over one QC-AAN training epoch on the entire MNIST dataset with  $N = 60,000$  images, we perform an update of the QCBM parameters every 100 batches for the simulation and every 600 batches for the experimental implementation. The latter implies one training step per training epoch. We use the Simultaneous Perturbation Stochastic Approximation (SPSA) algorithm [34] for training the parametrized quantum

circuit to adapt the model distribution of the QCBM while minimizing calls of the quantum device. The gradients are evaluated with 1000 readout measurements (shots). For the experimental implementation on the quantum device, we sample the 8 qubit distributions with  $10^4$  shots per measured basis and are able to construct multi-basis samples appropriately by resampling those measurements until the next training step. For the numerical simulations, this resampling was not performed and circuits were evaluated with as many shots as required for the GAN, i.e. for each image generated by the generator.

One technique that has shown to stabilize training for the QC-AAN is to freeze the prior, i.e. to fix the QCBM parameters, after a certain number of training epochs. Altering the prior distribution significantly in the latter stages of training has shown to destabilize training and lead to visibly worse images. Throughout this work, we freeze the prior after 10 epochs.

#### Appendix H: QCBM and RBM in the AAN-Framework

Quantum Circuit Born Machines (QCBMs) are promising quantum generative models that offer global sampling of the encoded distribution without algorithmic overhead and additionally provides access to quantum measurements that may be beneficial in learning a strong model. One of those properties, which we leverage in this work, is the possibility to measure in additional bases. Still, one needs to weigh the costs and benefits for such a quantum model when Restricted Boltzmann Machines (RBMs) are light-weight generative models with efficient but local sampling algorithm. Ref. [14] shows that the AAN framework with an RBM modeling the Generator's prior could be improved by instead implementing a Quantum Boltzmann Machine. Finding the best hyperparameters for their respective models is a notoriously difficult task and comparing models across all possible hyperparameter combinations is in general unfeasible. In this work, we argue that, given a poor choice of hyperparameters and the same number of model parameters, RBMs can easily become unstable in our smooth learning protocol while our QC-AAN models retain their stability. Fig. 7 shows a QC-AAN and an AAN, both with 8-dimensional prior on the MNIST training set. The stable, well-configured results correspond to 1 gradient step per training instance of the QCBM or RBM. The unfavorable hyperparameter configuration corresponds to 5 gradient steps with equal hyperparameters elsewhere. A priori, a step size of 0.01 seems small enough that both of the hyperparameter options do not seem unreasonable. In fact, 1 step changes the prior very little relative to a uniform distribution and 5 steps too much. Figure 7 shows the downfall of the RBM with its native local sampling technique that can get stuck in certain distribution modes. If it does, further training of the AAN becomes impossible. The transition for a QCBM prior between two hyperparameter choices is smoother and indicates a potentially improved robustness of the QCBM model compared to the RBM model in the AAN framework.

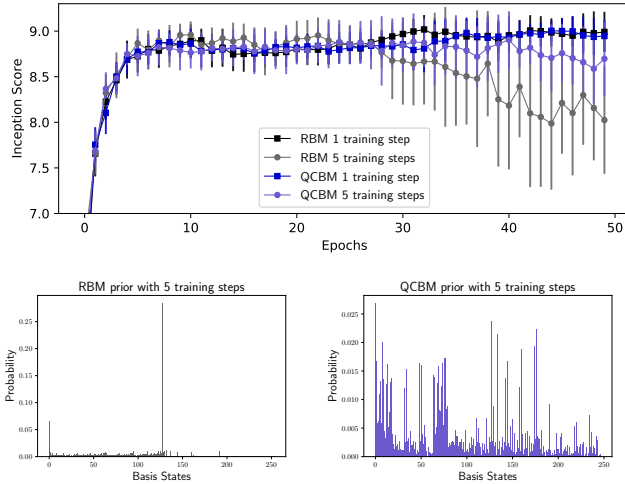


FIG. 7. Example comparison of two hyperparameter configurations for an AAN and QC-AAN, which implement a RBM and QCBM as the model prior, respectively. A training protocol of 5 training steps per training instance appears to be too much variation in the GAN prior for stable training, but unlike a QCBM, a RBM is prone to becoming unstable under sub-optimal configurations and sampling only one distribution mode. When that happens, training of the algorithm fails.

### Appendix I: Inception Score Definition & Discussion

The *Inception Score* (IS)

$$\text{IS}(G) = \exp(\mathbb{E}_{x \sim G}[\text{KL}(p(y|x) || p(y))]) \quad (\text{I1})$$

is a popular metric for evaluating GANs. For a given Generator  $G$ , it measures the quality  $p(y|x)$  of generated images  $x$  and also their diversity  $p(y)$  across all possible classes  $y$  of the original dataset. The IS is a human-readable metric with values between 1 and the number of total classes in the dataset, i.e. 10 for the MNIST dataset of handwritten digits. Although it has been proven to be very useful, one of the main criticisms of the IS is that it does not depict the realism of generated images for a human observer because it is calculated with classifiers which are trained to search and find exactly the class labels that they have been trained for. Images can either be warped or noisy and still achieve very high classification certainty [35]. In this work specifically, we achieve a surprisingly high IS with models that implement 6- and 8-dimensional priors, resulting in only 64 and 256 distinct images in total. Although the IS is high for those models, a human observer does not judge them as being particularly clear images. For such limited models, there arises an interesting effect where the discriminator can remember all images generated by the generator, constantly pushing it away, preventing further convergence and thus introducing noisy artifacts. Another classifier will clearly identify the digits as member of their particular class, regardless of the noise. Nevertheless, IS is a straight-forward quantitative performance measure for GANs that commonly correlates well with human perception.

The IS is commonly calculated with use of the pre-trained Inception-v3 Network [36] as a proxy to calculate the probabilities in Eq. I1. For this work, we instead utilize a convolutional classifier with approximately 99.3% accuracy on the MNIST data set.